

Geo-electrical Characterisation for CO₂ Sequestration in Porous Media

K.O. Rabiun, L.K. Abidoye[§], D.B. Das*

Chemical Engineering Department, Loughborough University, Loughborough, Leicestershire
LE11 3TU, United Kingdom

*Corresponding author (Email: D.B.Das@lboro.ac.uk)

[§]Current Address: Department of Civil Engineering, Osun State University, Osogbo, Nigeria

Running title: **Monitoring CO₂ Stored in Silicate, Carbonate and Basalt Media**

Abstract

Developing monitoring strategies for the detection and monitoring of possible CO₂ leakage or migration from existing and anticipated storage media are important because they can provide an early warning of unplanned CO₂ leakage from a storage site. While previous works have concentrated on silicate and carbonate porous media, this work explores geoelectrical techniques in basalt medium in a series of well-defined laboratory experiments. These were carried out to identify the key factors which affect geoelectrical monitoring technique of CO₂ in porous media using low cost and efficient time domain reflectometry (TDR). The system has been set up for simultaneous measurement of the bulk electrical conductivity and bulk dielectric permittivity of CO₂-water-porous media system in silica sand, basalt and limestone. Factors investigated include pH, pressure, temperature, salinity, salt type and the materials of the porous media. Results show that the bulk electrical conductivity and dielectric permittivity decrease as water saturation decreases. Noticeably, electrical conductivity and permittivity decrease due to the changes in water saturation and the relationship remains the highest in limestone except at the

24 start of the experiment. Also, an increase in temperature, pressure and salinity tend to increase
25 the bulk electrical conductivity (σ_b) and permittivity (ϵ_b) of the CO₂-water-porous media system
26 during the drainage experiment. On the other hand, pH and concentrations of different types of
27 salt do not seem to have significant effect on the geoelectrical characteristics of the system. It
28 was evident that Archie's equation fit the experimental results well and the parameters obtained
29 were in good agreement with those in the literatures. The regression shows a good reliability in
30 the prediction of electrical properties during the monitoring process of CO₂ sequestration.

31 **Keywords:** pH, electrical conductivity, dielectric permittivity, CO₂ leakage, water saturation.

32

33 **1 Introduction**

34 Carbon dioxide is known to be a major contributor to the greenhouse effect. It causes excessive
35 heating of the earth's atmosphere and, thus, contributes to the global climate change (Abidoeye et
36 al. 2014; Aliakbar et al. 2016; Mariyamma et al. 2015; Terzi et al. 2014). CO₂ emissions from
37 various sources such as power generation plants and automobiles have increased by more than
38 30 percent over the last decades (Bachu 2000; Metz et al. 2005; Shalek 2013; Socolow et al.
39 2004). Therefore, the removal of the emitted CO₂ is important to prevent the environmental disaster
40 such as change in precipitation patterns, the rise in sea levels, polar caps disruption, and acidic
41 oceans (Adefila and Yong 2013; Mariyamma et al. 2015). The approach of carbon capture and
42 sequestration (CCS) has been suggested to be one of the most promising ways of reducing the
43 present level of this emission into the atmosphere (Abidoeye et al. 2014; Folger 2009; Kilgallon
44 et al. 2014; Metz et al. 2005). Other methods include use of energy efficient system and
45 renewable energy but these techniques have been suggested to be less-effective when compared
46 to CCS (Abidoeye and Das 2015a; Alvarez 2014).

47 The CO₂ storage using CCS can be grouped into three categories: (i) geological storage; (ii)
48 mineralization; and (iii) ocean storage. The CO₂ geological storage (CGS) is considered as a

49 promising CO₂ sequestration method in developed countries; the geological formation includes
50 deep saline aquifer, unmineable coal deposits, depleted and mature oil and gas reservoirs while
51 the mineralization process is the conversion of CO₂ into solid inorganic carbonates during the
52 reaction of CO₂, brine and rock minerals. Mineralization method provides permanent storage of
53 CO₂; however, the conversion of CO₂ into solid carbonate is very slow while the high cost of
54 implementation is a concern (Druckenmiller and Maroto-Valer 2005).

55 The major problem of CO₂ storage in geological aquifer is the possible risk of CO₂ leakage from
56 the storage reservoir to shallower potable-water aquifer, which consequently may become a
57 threat to the living organisms (Abidoye and Das 2015b; Dafflon et al. 2013). The leakage may
58 be as a result of detrimental permeability pathways around the well or faulty caprock (Abidoye
59 and Das 2015b). But, if the reservoir is well characterised before CO₂ is injected, the problem of
60 leakages could be minimised. Khudaida and Das (2014) reported that injecting supercritical CO₂
61 into porous formations would minimise CO₂ leakage during geological sequestration of CO₂,
62 because storing CO₂ in supercritical phase will reduce the buoyancy, since the density of
63 supercritical CO₂ will be similar to that of brine (Khudaida and Das 2014). Also, monitoring of
64 CO₂ storage site before, during and after injection is very important for any CCS project
65 (Kilgallon et al. 2014) because this can provide an early warning of unplanned CO₂ leakage
66 from a storage site.

67 In the context of monitoring CO₂ sequestration, simultaneous measurement of electrical
68 conductivity and dielectric permittivity can provide accurate early warnings for the presence of
69 CO₂ in the water bodies, because an increase in CO₂ concentration signals a decrease in
70 geoelectrical properties (i.e., dielectric permittivity and electrical conductivity) as compared to
71 pure water (Abidoye and Das 2015a; Abidoye and Das 2015b). Previous works have been
72 conducted on the geoelectrical characterizations of CO₂-water/brine flow in porous media (see,
73 e.g., Abidoye and Das 2015a; Abidoye and Das 2015b; Lamert et al. 2012; Dethlefsen et al.

74 2013); however, these investigators did not exhaust the interplay of different factors that can
75 affect the behaviour of bulk electrical conductivity (σ_b) and bulk dielectric permittivity (ϵ_b) of
76 the fluid-fluid-solid system (i.e., CO₂-water-porous media system) in porous media, especially
77 in basalt medium. These factors include pressure and temperature of the system, in-situ fluid
78 salinity, materials of the porous medium, chemical characteristics of the in-situ salt (brine) and
79 soil pH.

80 Majority of the previous work on geophysical monitoring techniques utilised seismic methods,
81 electrical resistivity, borehole geophysics (see, e.g., Wagner 2016; Lamert et al. 2012; Schmidt-
82 Hattenberger et al. 2011; Bergmann et al. 2011; Borner et al. 2015). A limited number of
83 laboratory studies have focused so far on studying the effects of important parameters such as
84 temperature, salt composition, pH, fluid pressure and salinity on the monitoring techniques in
85 basalt, using bulk electrical conductivity (σ_b), dielectric permittivity (ϵ_b) and their respective
86 relationships with water saturation (S_w). While geo-electrical monitoring techniques can provide
87 an efficient and effective monitoring method (Lamert et al. 2012; Abidoye and Das 2015a;
88 Abidoye and Das 2015b), other geophysical monitoring techniques such as seismic are time
89 consuming and expensive (Zhang 2013).

90 Furthermore, the work of Wang and Tokunaga (2015) characterised CO₂ distribution, trapping
91 and leakage potential using capillary pressure - saturation relations. But their investigation was
92 conducted on limestone medium. Earlier, the works of Pentland et al. (2011) as well as Zuo and
93 Benson (2014) investigated CO₂ trapping in quartz-rich medium (sandstone). Similarly, the
94 works of Abidoye and Das (2015a, b) were based on silicate and carbonate media. Thus, it can
95 be inferred that most of the existing publications concentrate on silicate and carbonate porous
96 media. Meanwhile, Wang and Tokunaga (2015) are of the opinion that mineral contents of the
97 porous media determine the trapping capacity of the medium during geological carbon
98 sequestration. Basalt primarily consists of magnesium and calcium silicate minerals which

99 provide divalent metal cations necessary for the formation of solid carbonates (Matter and
100 Kelemen 2009; Snæbjornsdottir and Gislason 2016).

101 Therefore, question may be asked as to how basalt medium will affect CO₂ distribution, trapping
102 and leakage potential during geological carbon sequestration? This work explores this gap in
103 knowledge by investigating geoelectrical characteristics of CO₂-brine-porous medium system in
104 basalt medium as well as silicate and carbonate porous media.

105 This work determines the effects of temperature, pressure, pH, salinity, salt types and porous
106 material on geoelectrical characteristics of the CO₂-water-porous media system at high pressure
107 and temperature relevant to geological carbon sequestration. In addition to examining the
108 influence of porous media on the characteristics of CO₂-brine-porous media system, this work
109 also aims to investigate how inexpensive and effective time domain reflectometry (TDR) could
110 be used as tool for early detection of CO₂ migration in an engineered CO₂ storage reservoir.

111 **2 Methodology**

112 The laboratory experiment was designed to monitor the CO₂ level in porous media such as silica
113 sand, limestone and basalt. The characteristics of the samples used are described in Table 1. The
114 relationship between geo-electrical properties, i.e., bulk electrical conductivity and bulk
115 dielectric permittivity (σ_b and ϵ_b) and water saturation (S_w) makes it possible to monitor the
116 amount of CO₂ in the storage reservoir (Knight 1991, Abidoye and Das 2015a). Geological
117 conditions of CO₂ storage reservoirs, i.e., at high pressure and temperature relevant to geological
118 conditions, are to be mimicked in the experiments. The effects of various parameters such as
119 pressure, temperature, salt types, salt concentration, pH and porous material on the geo-
120 electrical monitoring performance were investigated.

121 Geo-electrical measurement techniques made use of locally fabricated three-pin time domain
122 reflectometry (TDR) probe and measured both dielectric permittivity and electrical conductivity,

123 simultaneously. TDR can measure electrical parameters simultaneously and was employed to
 124 acquire in-situ laboratory experimental data on σ_b and ϵ_b for CO₂-brine-porous media system in
 125 analogy to geological CO₂ sequestration in brine aquifer. In-situ experimental data acquired by
 126 the TDR were automatically transferred to the data acquisition system (CR10X datalogger,
 127 Campbell Scientific Ltd, Shepshed, UK).

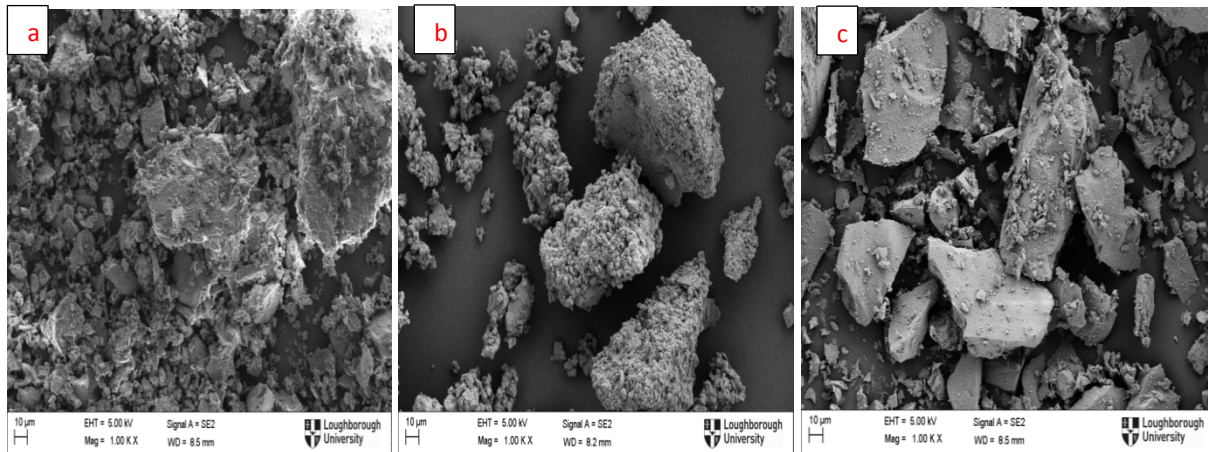
128 **2.1 Materials and Methods**

129 This work investigated three unconsolidated sand samples: silica sand (Minerals Marketing
 130 Company, Cheshire, UK), basalt sand (Aqua Maniac, Delaware, USA) and carbonate sand
 131 (limestone) (Tarmac Buxton Lime and Cement, Buxton, UK). The physical properties such as
 132 porosity, density, permeability, and average particle size of each mentioned porous materials
 133 were determined experimentally and are listed in Table 1. SEM (Zeiss 1530VP) images were
 134 taken before the experiment to examine surface morphology and roughness of the porous
 135 materials used. As shown in Figure 1, basalt sand has hexagonal shape; limestone has round
 136 shape while silica sand is more angular. All the sand materials were washed with tap/deionised
 137 water to remove excessive clay content.

138 **Table 1** Characteristics of the porous media used in the experiments

139 Parameters	Silica Sand	Carbonate sand	Basalt Sand
140 Porosity (%)	39±0.25	40±0.30	42±0.30
141 Intrinsic permeability (mD)	84±0.60	50±0.20	80±0.30
142 Average particle size (µm)	968±253	1147±270	1016±296

143



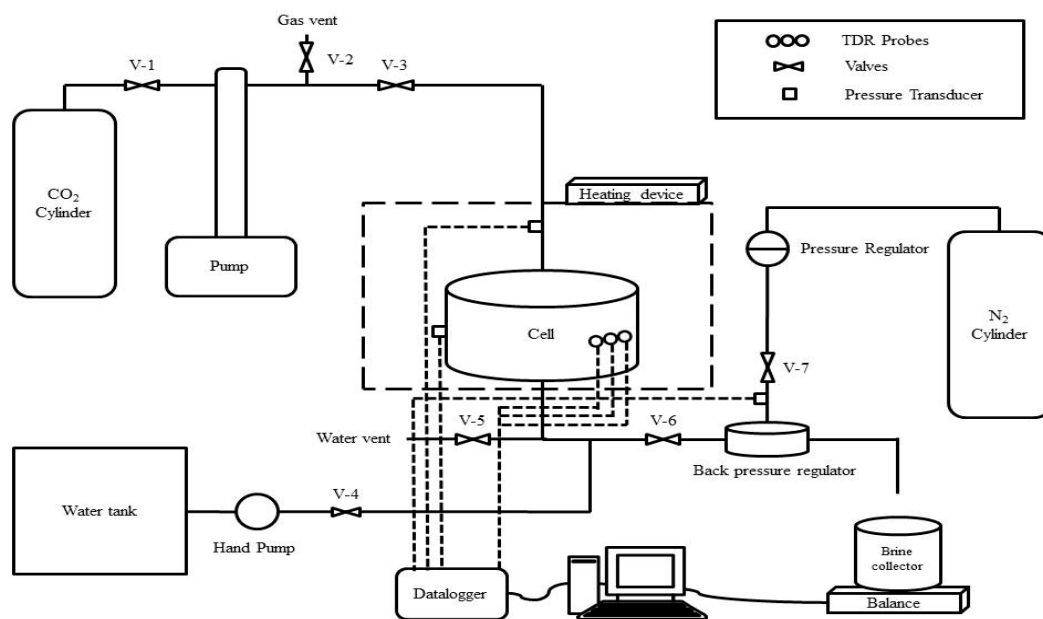
144
 145 **Fig. 1** Scanning electron microscope (SEM) images of: (a) Basalt; (b) Limestone; and (c)
 146 Silica sand particles
 147

148

149 **2.2 Set-up of the Experimental Rig**

150 The time domain reflectometry (TDR) equipment consists of three-pin probes which are held
 151 together with high temperature polytetrafluoroethylene (PTFE) that can withstand high pressure
 152 and temperature experimental conditions. The TDR probes cable was connected to a multiplexer
 153 that was attached to TDR100 reflectometer (Campbell Scientific Ltd, Shepshed, UK) and
 154 connected to CR10X datalogger (Campbell Scientific Ltd, Shepshed, UK). The 12V and 50 Hz
 155 dual rail power supply (Rapid Electronics Ltd, Essex, UK) supplied power to the CR10X
 156 datalogger. The data-acquisition system was connected to the desktop computer into which data
 157 were stored automatically from the TDR probes that were inserted into the porous material
 158 during the experiment. Before the start of any experiment, the TDR device was calibrated using
 159 Campbell Scientific Instruction manual and the acquired readings from the calibration were used
 160 in developing the program. This program was used by the TDR 100 reflectometer to
 161 communicate with the datalogger. Figure 2 shows a schematic diagram of the experimental rig
 162 used in this work. The pressure transducers (PTs) and the time domain reflectometry (TDR)
 163 probe were attached to the centre of the stainless steel cell (porous medium holder). The PTs
 164 measured the in-situ system pressure while the TDR measured the geo-electrical properties of

165 the saturated sand. The stainless steel chamber holding the saturated porous material was
 166 positioned in the heating cabinet having PID temperature controller (West Control Solutions,
 167 Brighton, UK) to regulate the system temperature. The steel sample holder had dimensions of 4
 168 cm height and 10 cm diameter with top and bottom end-pieces that were made of stainless steel.
 169 The inner part of the top end piece was overlain with hydrophobic polytetrafluoroethylene,
 170 PTFE (0.1 μm) and the bottom end piece with hydrophilic nylon (1 μm). The membranes were
 171 obtained from Porvair Filtration Group Ltd (Hampshire, UK). It has been reported that a
 172 hydrophilic membrane minimizes scCO_2 escape from the bottom of the sample holder, while
 173 hydrophobic membrane was used to reduce the inflow of water into the scCO_2 pump (Abidoye
 174 and Das 2015a).



175
 176 **Fig. 2** A schematic diagram of the experiment rig

177
 178 Moreover, a metering valve (Swagelok, Kings Langley, UK) was used for smooth flow control
 179 of water/brine from the experimental rig into the water collector situated on the measuring
 180 weigh balance. Back pressure regulator (BPR) (Equilibar, Fletcher, USA) was also connected to

181 the system and this maintained the system by stabilizing the outflow of the water/brine at the set
182 pressure. The back pressure regulator was loaded with nitrogen gas from a nitrogen cylinder
183 (BOC gases, Leicester, UK).

184

185 **2.3 Experimental Methods**

186 All experiments were conducted in a fabricated stainless steel of 4 cm height and 10 cm
187 diameter. The sample holder was placed on the bottom end piece with overlaying of the
188 hydrophilic membrane and tightens the bolt firmly to avoid leakage. Brine water is prepared in
189 the laboratory by mixing distilled water and sodium chloride salt obtained from Fisher Scientific
190 (Loughborough, UK). For other salt, namely, magnesium chloride (Fisher Scientific,
191 Loughborough, UK) used in this work, a similar procedure was observed. Equation (1) was used
192 for preparing solutions of different brine concentrations. The salt concentrations used in this
193 work were 0% w/w, 0.5 %w/w and 2 % w/w, respectively.

$$194 \quad \% w/w = \frac{\text{mass of solute}}{\text{mass of solution}} \times 100 \quad (1)$$

195 Small quantity of brine water was poured into the domain and the measured sand was passed
196 through a metal sieve of appropriate size. Same quantity of sand (500g) was used in all the
197 experiments. Thereafter, more brine water was added to make the porous media saturated. It was
198 ensured that the sand was well compacted and the cell was covered by the stainless steel top end
199 piece overlain with the hydrophobic membrane. All the joint bolts were tightened very well to
200 avoid any leakage during the experiment. Before starting each experiment, the pH of brine water
201 collected from saturated porous media was measured with a pH meter (Jenway, Fisher
202 Scientific, Loughborough). For example, the initial pH of saturated basalt sand is 6.5 ± 0.2 . For
203 the experiments at different pH, i.e., pH 12, the pH of the saturated rock media was adjusted to
204 pH 12.0 ± 0.2 using 0.02 M NaOH. Carbon dioxide (99.9% purity) used in this work was

205 purchased from BOC gases (Leicester, UK). The ScCO₂ fluid pump (Teledyne Isco, Lincoln
 206 NE) was set to refill mode and filled with liquid CO₂ from the CO₂ cylinder by opening valve 1
 207 (V-1; Figure 1). Afterward, V-1 was closed and the ScCO₂ fluid pump was set to the
 208 experimental pressure. The heater was switched on and also set at the experimental temperature.
 209 When temperature and pressure reached the predetermined values, i.e., when there was
 210 equilibrium in experimental condition (both temperature and pressure), V-3 and V-6 were
 211 opened (see Figure 1) and the displacement of brine began by CO₂. The experiment was stopped
 212 when there was no more brine coming out of the porous media sample in the sample holder
 213 (steel cell). Then, the porous media sample was removed from the cell for subsequent
 214 experiment. The sand removed from the cell was recycled by washing it with large volume of
 215 tap or deionized water. Table 2 shows the experimental conditions that mimic the geological
 216 conditions in which CO₂ is being stored.

217 **Table 2** Experimental conditions that were utilized in this work

218	S/n	Pressure (bar)	Temperature (°C)	CO ₂ Phase
219	1	65	23	Liquid CO ₂
220	2	75	23	Liquid CO ₂
221	3	75	35	ScCO ₂
222	4	90	35	ScCO ₂

223

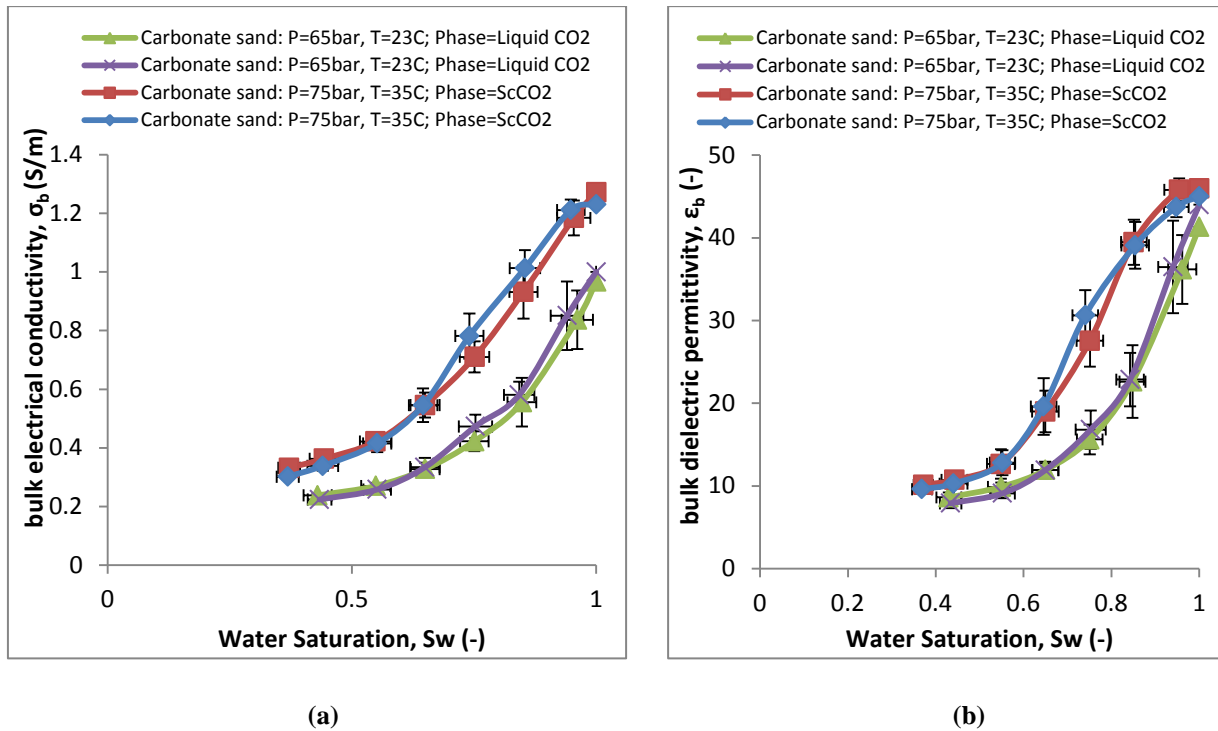
224 **3 Results and Discussion**

225 **3.1 Electrical Conductivity and Dielectric Permittivity**

226 Electrical conductivity and dielectric permittivity have functional relationships with water
227 saturation (Plug et al. 2007; Abidoeye et al. 2014; Abidoeye and Das 2015a) and these can be used
228 in monitoring the quality of fluids in the reservoir.

229 Our study focused on the effects of salt types, pH, porous material, salinity, pressure and
230 temperature on the geoelectrical characteristics of CO₂-brine-porous media system. The results
231 of various factors investigated in connection with the σ_b -S and ϵ_b -S relationships for scCO₂-
232 brine-porous media system are discussed below.

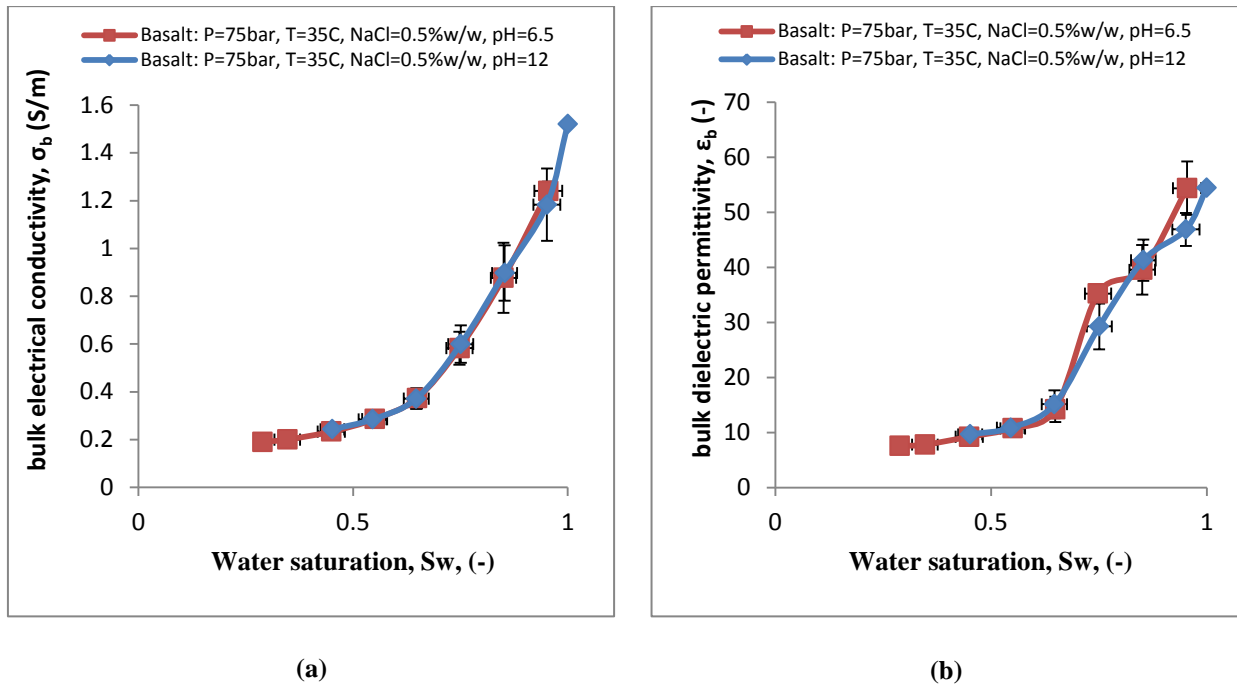
233 Figures 3a and 3b show that the experiments are repeatable under different injection conditions
234 corresponding to both liquid CO₂ and supercritical CO₂. The figures show results from two
235 separate measurements for σ_b -S and ϵ_b -S relationships under similar conditions for both liquid
236 CO₂ and scCO₂. The figures further show that the ϵ_b -S and σ_b -S relationships are functions of
237 water saturation as indicated by the fact that they decrease as the water saturation reduces. For
238 the σ_b -S relationship (Figure 3a), the decrease in σ_b -S relationship might be as a result of water
239 being a better conductor of electricity than CO₂. For the case of ϵ_b -S relationship (Figure 3b),
240 the decrease in permittivity and water saturation trend should be connected with the high
241 permittivity of water compared to CO₂ (Drnevich et al. 2001).



242 **Fig. 3** Repeatability plot for (a) σ_b - S and (b) ϵ_b - S relationships for liquid CO_2 / ScCO_2 – water - carbonate sand
 243 system
 244

245 **3.2 Effect of pH on Geo-electrical Properties**

246 It has been reported that pH has effects on mineralisation (Druckenmiller and Maroto-Valer
 247 2005; Liu and Maroto-Valer 2011). High pH is considered to speed up the mineralisation and it
 248 can be expected that this will affect the geoelectrical properties of the system. However, our
 249 work shows that there is no significant effect of pH. This is probably owing to the short time of
 250 the experiment during which significant mineralisation might not have occurred. Presumably, if
 251 the experiment was left for longer period of time, there might be a significant effect of
 252 mineralization and change in pH on the measured geoelectrical characteristics of CO_2 -water-
 253 porous media system. Figures 4a, b display the results of pH effects on the σ_b - S and ϵ_b - S
 254 relationships in basalt sand. At different pH values, e.g., 6.5 and 12, pH does not have any
 255 significant effect on the ϵ_b - S and σ_b - S relationships. Although, according to Abidoye and Das
 256 (2015b), pH has effect on conductivity under static conditions, when dissolution is higher, but
 257 the flow condition in this work does not reveal similar effect.



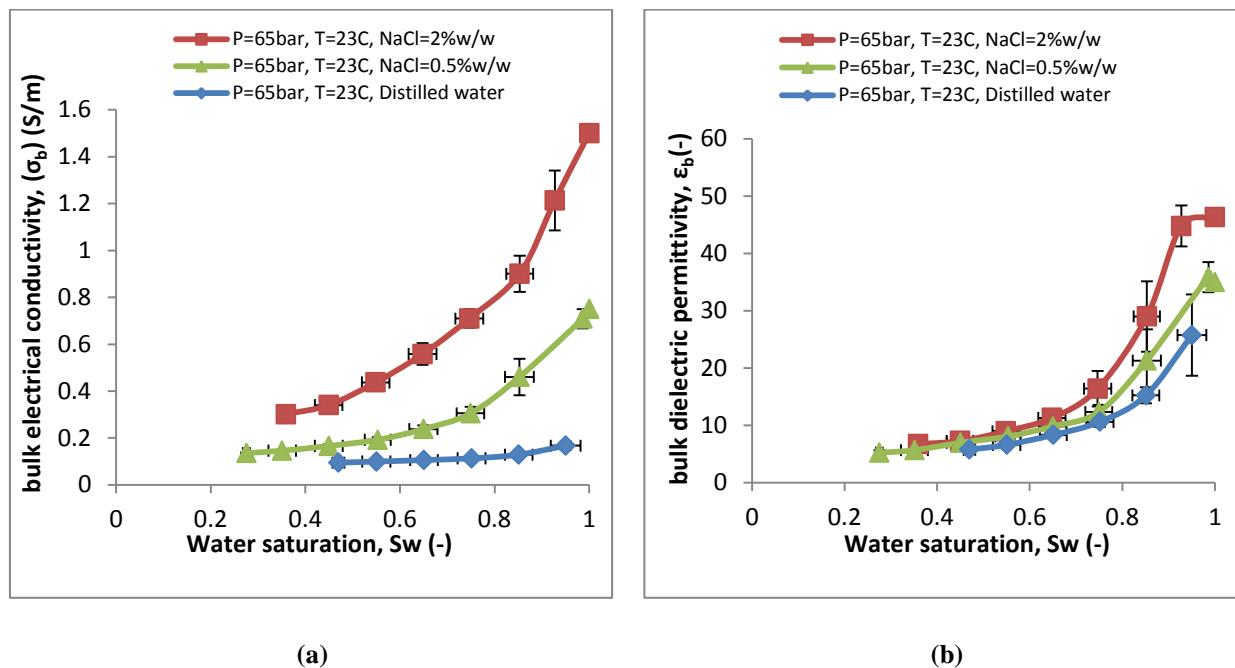
258 **Fig. 4** Effect of pH on (a) σ_b - S and (b) ϵ_b - S relationships for CO₂-water-basalt sand system

259

260 3.3. Effect of Salt Concentration

261 All saline aquifers contain brackish water and the amounts of salt concentration in them vary
 262 depending on their locations, i.e., concentrations between 0.5 and 153 g/L are found in most of
 263 the deep saline aquifers (Abidoye et al. 2014; Abidoye and Das 2015a; Buttinelli et al. 2011).
 264 The effects of salt concentration on geoelectrical properties and water saturation (σ_b - S and ϵ_b - S
 265 relationships) are examined in this study. The σ_b - S and ϵ_b - S relationships at different salt
 266 concentrations in silica sand are shown in Figures 5a, b. As expected, σ_b and ϵ_b increase with the
 267 increase in salt concentration. The increases in σ_b and ϵ_b values correspond to the increase in
 268 ions as salinity increases. This trend is more significant in the σ_b - S relationships (Figure 5a).
 269 However, for the ϵ_b - S curves (Figure 5b), there is only a slight change with different salt
 270 concentrations. The sensitivity of σ_b - S relationship to change in salt concentration can be
 271 attributed to the increase in ions in aqueous solution which raise the conductivity of the system.
 272 Furthermore, the figures reveal that the salt concentration is an important factor when compared

273 to distilled water having less aqueous ions. The σ_b -S relationship increases when the
 274 concentration of brine is raised to 0.5 %w/w (NaCl) and the trend further increases when the
 275 concentration of the brine increases to 2 %w/w (NaCl). The results are similar to the results
 276 from Abidoye and Das (2015a), but they limited their work to σ_b -S relationships only. The
 277 current work focuses on simultaneous measurement of σ_b -S and ϵ_b -S relationship in porous
 278 materials.

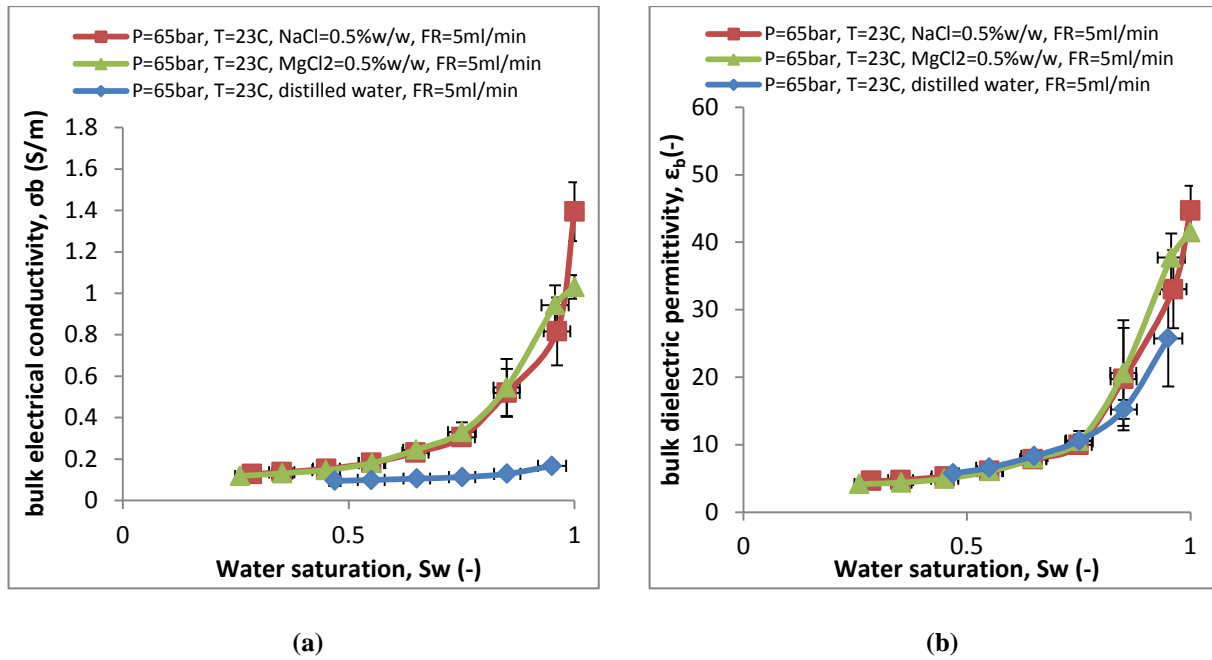


279 **Fig. 5** (a) σ_b -S and (b) ϵ_b -S relationships at different salt concentrations for liquid CO_2 in silica sand

280

281 3.4 Effect of Salt Types

282 The effect of salt types on σ_b -S and ϵ_b -S relationships in silica sand was also studied. Figures 6a
 283 and 6b display the influences of salt types on geoelectrical properties (σ_b , ϵ_b) and water
 284 saturation (S_w). It can be deduced that salt types do not have any significant effects on
 285 geoelectrical properties (σ_b , ϵ_b) and water saturation relationships when similar concentrations of
 286 different salt types (NaCl and $MgCl_2$) are used. This is clear from the figures; the only shifts in
 287 the curve occur when compared with distilled water. Thus, different salt types have similar
 288 effects on the σ_b -S and ϵ_b -S relationships.



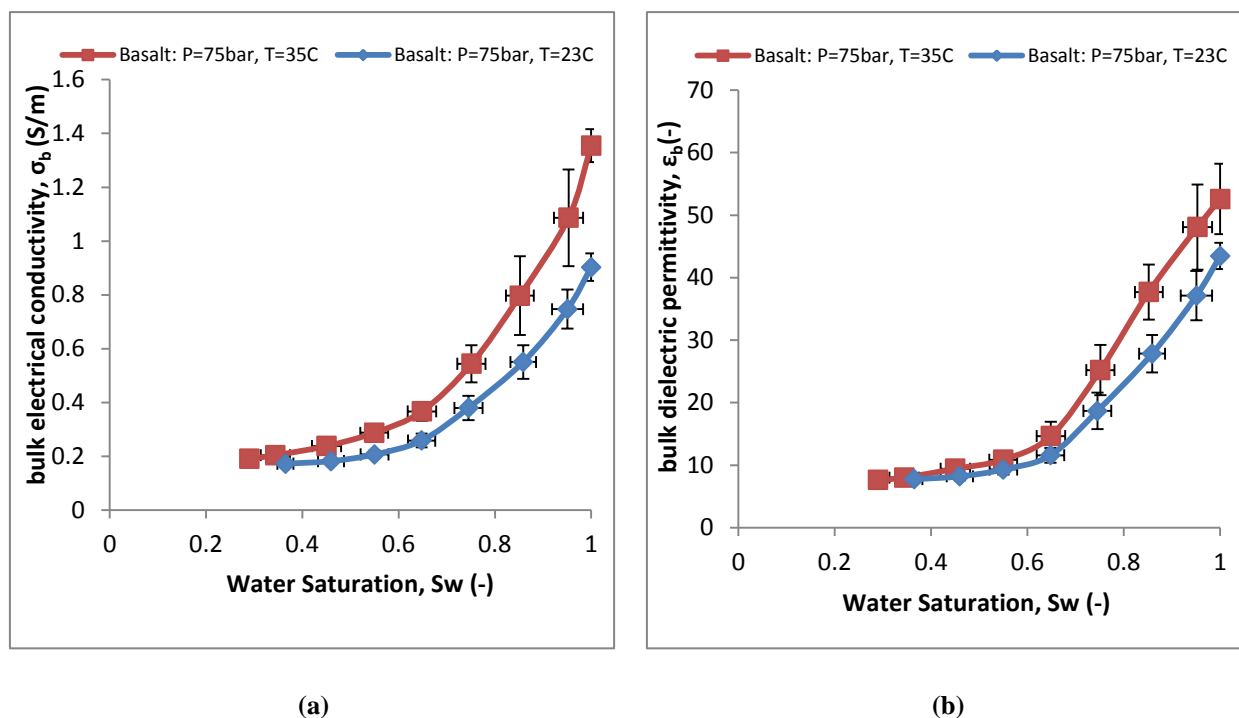
289 **Fig. 6** (a) σ_b - S and (b) ϵ_b - S relationships for different salt types for liquid CO_2 in silica sand
 290

291 3.5 Effect of Temperature

292 In the earth's crust, pressure and temperature gradually increase with depth. The geothermal
 293 gradient and hydrostatic pressure vary depending on the locations. Generally, CO_2 is stored at
 294 the depth of 800 to 1000 metres and at this depth the pressure is about 75 bar and the
 295 temperature is about 34°C (Abidoeye et al., 2014). At these conditions, CO_2 is in supercritical
 296 phase. In this work, the impact of temperature on the σ_b - S and ϵ_b - S relationship was investigated
 297 and the results are shown in Figures 7a and 7b, respectively. It is found that the σ_b and ϵ_b
 298 increase as the temperature increases in basalt sand system. Similar work on the effect of
 299 temperature on geoelectrical properties and water saturation relationship has been carried out on
 300 silica sand and limestone sand (Abedian and Baker 2008; Or and Wraith 1999; Abidoeye and Das
 301 2015a) but the current work utilises basalt sand because it is assumed that mineralisation takes
 302 place in basalt sand more rapidly than silica and carbonate sand media (Petrik and Mabee 2011).
 303 This may be the reason that Snæbjörnsdóttir et al. (2014) explored the permanency and potential
 304 of storing significant amount of CO_2 in basaltic rocks during carbon sequestration (Petrik and

305 Mabee 2011; Matter and Kelemen 2009; Snæbjörnsdóttir et al. 2014; Snæbjörnsdóttir and
306 Gislason 2016).

307 The result in Figure 7a shows that an increase in temperature tends to increase the electrical
308 conductivity (σ_b). This is possibly due to increase in the mobility of ions or the dissolution of the
309 medium at higher temperature. Also, increase in temperature results in increase in permittivity
310 (ϵ_b) and this can be attributed to the release of bound water, as claimed by Or and Wraith (1999).
311 The same trend for ϵ_b -S has been observed by Drnevich et al. (2001) for clay but they observed
312 decrease in dielectric permittivity with increasing temperature in sandstone (Drnevich et al.
313 2001; Or and Wraith, 1999).



314 Fig. 7 Effects of temperature on (a) σ_b -S and (b) ϵ_b -S relationships for CO₂-water-basalt sand system

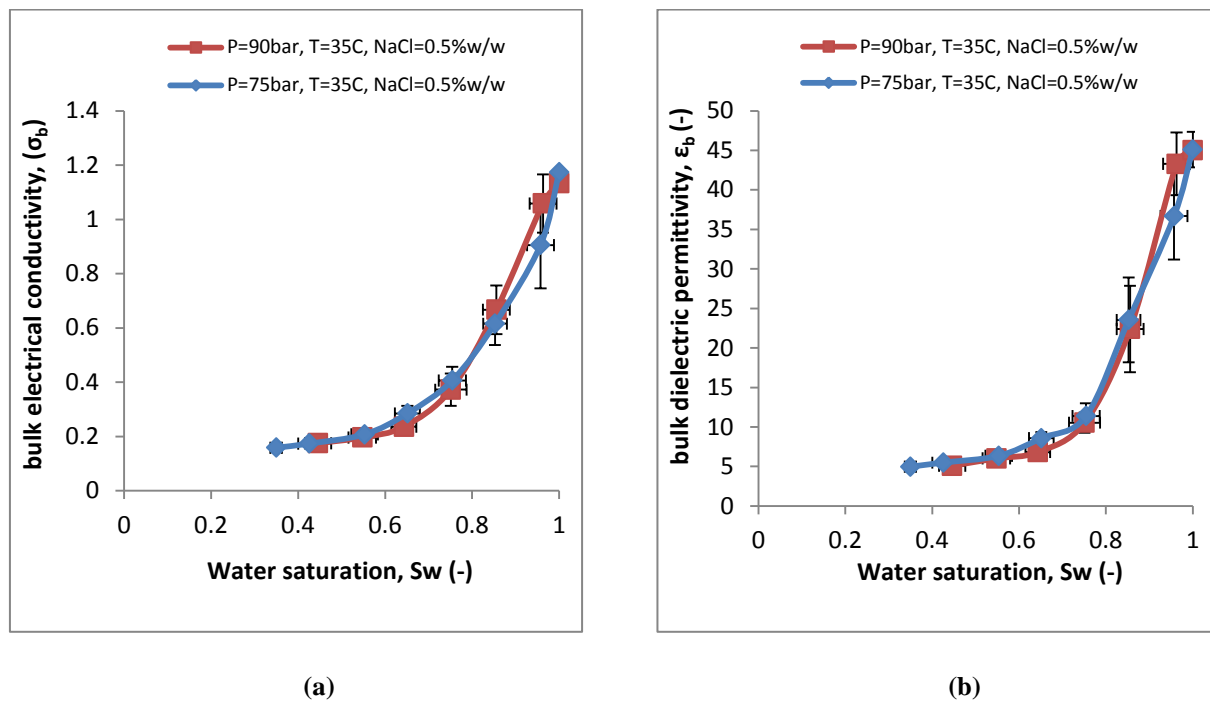
315

316 3.6 Effect of Pressure

317 It is paramount to understand the effect of pressure on the geoelectrical characteristics of scCO₂-
318 water-sand system, because geological carbon sequestration takes place at different depths.
319 Different injection pressures that correspond to varying injection depths were used in the

320 laboratory to simulate these different injection conditions. Figures 8a and 8b show the
 321 relationships between geoelectrical properties (ϵ_b and σ_b) and water saturation. The results
 322 revealed that ϵ_b -S and σ_b -S relationships increase slightly with increasing pressure especially at
 323 higher water saturation (80% and above) for σ_b -S relationships; and 90% and above for ϵ_b -S
 324 relationships.

325



326 **Fig. 8** Effects of pressure on (a) σ_b -S and (b) ϵ_b -S relationships in ScCO₂-water-silica sand system

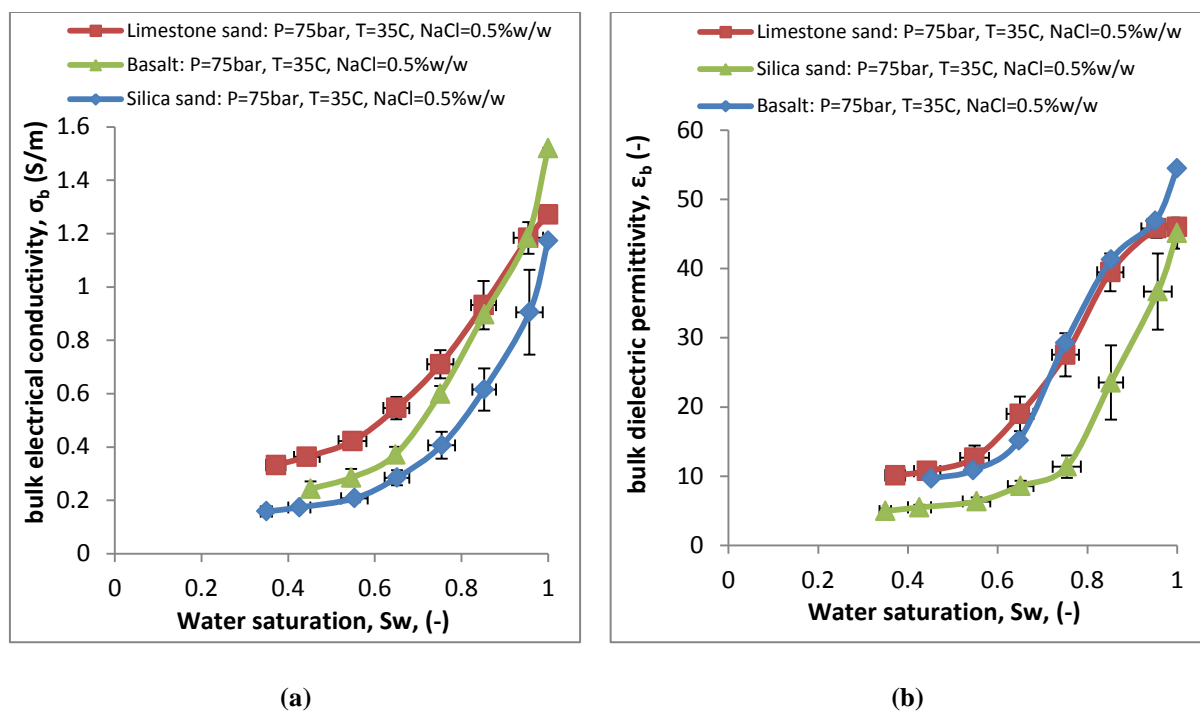
327

328

329 3.7 Effect of Rock Type

330 Figures 9a and 9b show the effect of porous materials on ϵ_b -S and σ_b -S relationships. It can be
 331 deduced that the type of rock present in the porous rock body has a noticeable effect on both the
 332 σ_b -S and ϵ_b -S curves. Abidoye and Das (2015a) attribute the high conductivity in the (carbonate
 333 sand) limestone-water-CO₂ system to the dissolution of carbonate sand in water with subsequent
 334 increase in concentration of dissolved ions (Plan 2005; Assayag et al. 2009). Figures 9a and 9b

335 show the σ_b - S and ϵ_b - S relationships for different rock types (i.e., basalt, carbonate and silica
 336 sand). In the σ_b - S relationship, the curve is highest than others for limestone, except at the start
 337 of the experiment. At the start of the experiment, basalt sand is shown to have higher σ_b - S curve
 338 (i.e., at saturation of 1) than carbonate and silica sand, respectively. The explanation for this is
 339 that at the start of the experiment ($S_w=1$), less limestone has dissolved, thus the limestone
 340 presence does not affect σ_b - S at this time. After some time, more dissolution has occurred. Since
 341 dissolution of carbonate is higher than others, electrical properties may be more affected in
 342 carbonate than others. This was also observed by Abidoye and Das (2015a) but their work was
 343 limited to only carbonate and silica sand. The current study utilises three porous materials, i.e.,
 344 basalt, carbonate and silica sand. It is concluded that different porous materials behave
 345 differently on geoelectrical properties and water saturation relationships.



346 **Fig. 9** Effect of porous media samples on (a) σ_b - S and (b) ϵ_b - S relationships in scCO_2 - water silica/limestone/
 347 basalt sand system

348 **3.8 Regression of the Experimental Result**

349 This section discusses the results of the geoelectrical parameters (σ_b and ε_b) for scCO₂-
350 water/brine system. An attempt was made to fit the experimental results to Archie's law
351 (Archie 1942), and thus, predict the bulk conductivity σ_b in the silica sand, basalt sand and
352 limestone. Archie's equation can be written in terms of conductivity as follows:

$$353 \quad \sigma_b = \frac{S^n}{\phi^{-m}} \sigma_w \quad (2)$$

354 where,

355 S = water saturation, ϕ = porosity, σ_w = brine conductivity, σ_b = bulk conductivity,
356 m = cementation exponential, n = saturation exponential.

357 The equation can be used to fully predict water saturation (S) from porosity (ϕ), brine
358 conductivity (σ_w) and bulk conductivity (σ_b) measurements. Also, adjustable parameters m
359 and n are the Archie's empirical parameters, which depend on formation characteristics and are
360 used for the optimization of the model (Kennedy and Herrick 2012). From the silica, basalt and
361 carbonate sand used in this work, the exponents m and n were determined from the
362 experiments. Equation (2) was linearized using logarithm rules to form Eqs. (3) and (4). XLfit
363 was then used to solve for m and n exponents.

$$364 \quad \log \sigma_b - m \log \phi = \log \sigma_w + n \log S \quad (3)$$

$$365 \quad n \log S + m \log \phi = \log \sigma_b - \log \sigma_w \quad (4)$$

366 Table 3 shows the values of m and n exponents using Microsoft XLfit.

367

368

369

370 **Table 3** Archie's (1942) exponents and correlation coefficients (R^2) for each of the porous material
371 tested

372

373	Porous media sample	n	m	R^2
374	Limestone	1.1	2.0	0.87
375	Silica sand	0.8	1.7	0.75
376	Basalt sand	0.9	1.8	0.70

377 The exponent values in Table 3 are in good agreement with the reports from the literature.
378 Values of 1.0 to 2.2 were reported for both m and n exponents in carbonates and sandstones
379 (Scudiero et al. 2012; Wang et al. 2014). According to Abidoye and Das (2015a), the values of
380 m for sandstone and carbonate are 1.2 and 1.4, respectively. Also, n has the value of 1.2 and 1.5
381 for silica sand and carbonate sand, respectively (Abidoye and Das 2015a). On the other hand,
382 Scudiero et al. (2012) give the range between 1.3 to 2.5 for the values of m, and n value to be
383 2.0. In addition, Liu and Moysey (2012) give the range between 0.7 and 1.96 for n value. It can
384 be concluded that the exponent values for m and n from the model generated from our
385 experiment is similar to others.

386 Additionally, the bulk dielectric permittivity (ϵ_b) is a function of various parameters, such as
387 water saturation (S), pressure (P), temperature (T), and the initial value of ϵ_b (i). The initial value
388 of ϵ_b is the value of dielectric permittivity of porous materials saturated with water before
389 injection of CO₂. This value of ϵ_b is very crucial, because it shows the original state of water
390 saturated medium, which eventually determines the ϵ_b -S profile. Therefore, ϵ_b can be written
391 as:

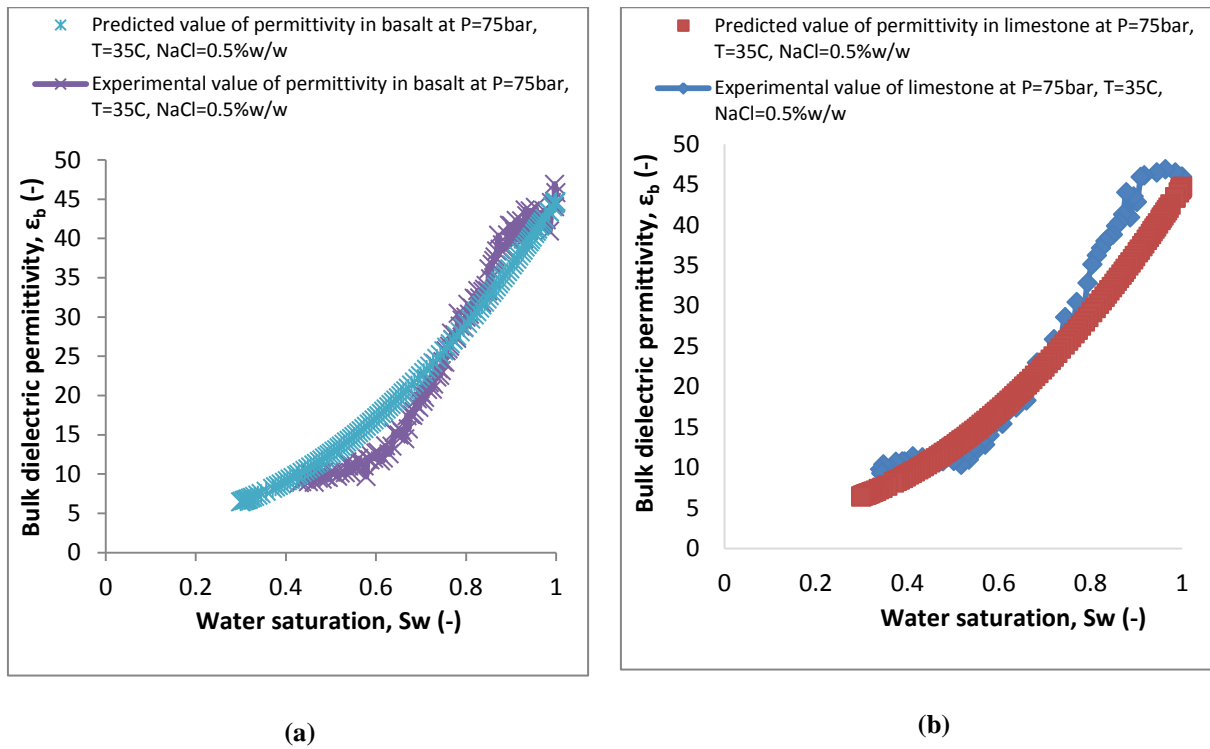
392
$$\epsilon_b = f(S, P, T, i) \tag{5}$$

393 The Minitab statistical software (Microsoft 2016) was used to determine dielectric permittivity
394 (ϵ_b). The nonlinear regression polynomial model is shown as Eq. (6):

395 $\epsilon_b = -47.11 - 7.69S - 0.0057P + 1.156T + 0.237i + 47.94S^2$ (6)

396 The results of the regression using Eq. (6) are shown in Figures 10a and 10b. The figures show
 397 that the model is in agreement with the observed values because they capture most of the data
 398 accurately. It can be hypothesised that the nonlinear regression presented in this work using fit
 399 regression model is very reliable in predicting ϵ_b - S relationship for two-phase flow in porous
 400 media. This model can be used to predict the monitoring process of CO₂ sequestration.

401



402 **Fig. 10** Prediction of permittivity values in (a) CO₂-water-basalt and (b) CO₂-water-limestone systems at 75bar and
 403 35⁰C using non-linear regression

404

405 4. Conclusions

406 Monitoring CO₂ in geological storage reservoir is crucial in the context of carbon capture and
 407 sequestration. To this end, this work explored the effects of pressure, temperature, salt types,

408 salinity, pH and porous media on the geo-electrical characteristics of the CO₂-water-porous
409 media flow system, with a view to enhancing effective subsurface monitoring of the system.
410 Time domain reflectometry (TDR) method was used for simultaneous analysis of the in-situ
411 characteristics of the bulk dielectric permittivity and electrical conductivity for CO₂-water-
412 porous media system, for liquid and supercritical CO₂ in silica sand, basalt sand and carbonate
413 sand. The bulk electrical conductivity and dielectric permittivity decrease as water saturation
414 decreases in the porous media. Results show that an increase in temperature, pressure and
415 salinity tend to increase the bulk electrical conductivity (σ_b) and permittivity (ϵ_b) relationships
416 with in-situ water saturation. On the other hand, pH and salt types do not show any significant
417 effect on the geoelectrical parameters (σ_b , ϵ_b). Effects of porous materials on both the bulk
418 electrical conductivity and permittivity curves show that the profile values are highest in
419 limestone medium, followed by basalt and then silica sand, under similar conditions. This effect
420 can be attributed to the different chemical compositions contained in silica, carbonate and basalt
421 sand media. Archie equation using XLfit (Microsoft 2016) was used to model the experimental
422 results and the outputs were in good agreement with previous studies. In addition, a polynomial
423 fit developed in this study took into consideration the other parameters such as pressure,
424 temperature and initial bulk permittivity. The fit regression model shows a good reliability in the
425 prediction of geoelectrical characteristics of the system during the monitoring process of the
426 geological CO₂ sequestration.

427

428 **References**

429 Abedian B, Baker KN (2008) Temperature effects on the electrical conductivity of dielectric
430 liquids. *IEEE Transactions on Dielectrics and Electrical Insulation*, 15, 888–892.
431 <http://doi.org/10.1109/TDEI.2008.4543127>

- 432 Abidoye LK, Das DB (2015a) Geoelectrical characterization of carbonate and silicate porous
433 media in the presence of supercritical CO₂–water flow. *Geophys. J. Int.* 203, 79–91
- 434 Abidoye LK, Das DB (2015b) pH, geoelectrical and membrane flux parameters for the
435 monitoring of water-saturated silicate and carbonate porous media contaminated by CO₂.
436 *Chem. Eng. J.* 262, 1208–1217
- 437 Abidoye LK, Khudaida KJ, Das DB (2014) Geological Carbon Sequestration in the Context of
438 Two-Phase Flow in Porous Media: A Review. *Crit. Rev. Environ. Sci. Technol.* 45, 1105–
439 1147
- 440 Adefila K, Yong Y (2013) A compendium of CO₂ leakage detection and monitoring techniques
441 in carbon capture and storage (CCS) pipelines. *Eurocon, 2013 Ieee* 1328–1335
- 442 Aliakbar K, Ali V, Mohammadreza R, Reza A (2016) Carbon Dioxide Geological Storage
443 (CGS) – Current Status and Opportunities. In: Moya BL and Pous J (eds) *Greenhouse*
444 *Gases* doi:10.5772/62173. Available at: [https://www.intechopen.com/books/greenhouse-](https://www.intechopen.com/books/greenhouse-gases/carbon-dioxide-geological-storage-cgs-current-statusand-opportunities)
445 [gases/carbon-dioxide-geological-storage-cgs-current-statusand-opportunities](https://www.intechopen.com/books/greenhouse-gases/carbon-dioxide-geological-storage-cgs-current-statusand-opportunities)
- 446 Alvarez AG (2014) Methodologies to detect leakages from Geological carbon storage sites.
447 Department of Civil and Environmental Engineering, Colorado State University, Fort
448 Collins, Colorado (PhD thesis)
- 449 Archie G (1942) The electrical resistivity log as an aid in determining some reservoir
450 characteristics. *Transaction of the american institute of mining and metallurgical engineers*,
451 146, pp. 54–61
- 452 Assayag N, Matter J, Ader M, Goldberg D, Agrinier P (2009) Water–rock interactions during a

453 CO₂ injection field-test: Implications on host rock dissolution and alteration effects,
454 Chemical geology, 265, pp. 227–235. <http://dx.doi.org/10.1016/j.chemgeo.2009.02.007>

455 Bachu S (2000) Sequestration of CO₂ in geological media: criteria and approach for site
456 selection in response to climate change. *Energy Convers. Manag.* 41, 953–970

457 Bergmann P, Yang C, Lüth S, Juhlin C, Cosma C (2011) Time-lapse processing of 2D seismic
458 profiles with testing of static correction methods at the CO₂ injection site Ketzin
459 (Germany). *J. Appl. Geophys.* 75, 124–139,
460 <http://dx.doi.org/10.1016/j.jappgeo.2011.05.005>

461 Borner JH, Herdegen V, Repke J, Spitzer K (2015) The electrical conductivity of CO₂-bearing
462 pore waters at elevated pressure and temperature: a laboratory study and its implications in
463 CO₂ storage monitoring and leakage detection. *Geophys. J. Int.* 203, 1072–1084
464 doi: 10.1093/gji/ggv331

465 Buttinelli M, Procesi M, Cantucci B, Quattrocchi F, Boschi E (2011) The geo-database
466 of caprock quality and deep saline aquifers distribution for geological storage of CO₂ in
467 Italy, *Energy*, **36**(5), 2968–2983

468 Dafflon B, Wu Y, Hubbard SS, Birkholzer JT, Daley TM, Pugh JD, Peterson JE, Trautz RC
469 (2013) Monitoring CO₂ intrusion and associated geochemical transformations in a shallow
470 groundwater system using complex electrical methods. *Environ. Sci. Technol.* 47, 314–321

471 Dethlefsen F, Kober R, Schafer D, Hagrey SAA, Hornbruch G, Ebert M, Dahmke A (2013)
472 Monitoring Approaches for Detecting and Evaluating CO₂ and Formation Water Leakages
473 into Near-surface Aquifers. *Energy Procedia*, 37, pp.4886–4893

474 Drnevich VP, Yu X, Lovell J, Tishmack J, Zhang, J (2001) BTemperature effects on dielectric
475 constant determined by time domain reflectometry, ^ TDR 2001: Innovative Applications of
476 TDR Technology, Infrastructure Technology Institute, Northwestern University, Evanston,
477 IL, September 5-7, 2001. Available at: [http://www.iti.northwestern.](http://www.iti.northwestern.edu/tdr/tdr2001/reviewers/subgrade_monitoring/drnevich3/Drnevich3.pdf)
478 [edu/tdr/tdr2001/reviewers/subgrade_monitoring/drnevich3/Drnevich3.pdf](http://www.iti.northwestern.edu/tdr/tdr2001/reviewers/subgrade_monitoring/drnevich3/Drnevich3.pdf). Accessed 30
479 May 2016

480 Druckenmiller ML, Maroto-Valer MM (2005) Carbon sequestration using brine of adjusted pH
481 to form mineral carbonates. *Fuel Process. Technol.* 86, 1599–1614

482 Folger P (2009) Carbon Capture and Sequestration (CCS).
483 <http://digitalcommons.unl.edu/cgi/viewcontent.cgi?article=1043&context=crsdocs>

484 Kennedy DW, Herrick DC (2012) Conductivity models for Archie rocks. *Geophysics* 77(3),
485 WA109–WA128. doi:10.1190/geo2011-0297.1

486 Khudaida KJ, Das DB (2014) A numerical study of capillary pressure-saturation relationship for
487 supercritical carbon dioxide (CO₂) injection in deep saline aquifer. *Chem. Eng. Res. Des.*
488 92, 3017–3030

489 Kilgallon R, Gilfillan S, McDermott C, Edlmann K, Haszeldine S (2014) Investigating the role
490 of noble gases as tracers for CO₂ storage. *Energy Procedia* 63, 4172–4179

491 Knight R (1991) Hysteresis in the electrical resistivity of partial saturated sandstones.
492 *Geophysics*, 56, pp. 2139 – 2147.
493 [https://pangea.stanford.edu/research/enviro/papers/Knight%20\(1991\).pdf](https://pangea.stanford.edu/research/enviro/papers/Knight%20(1991).pdf)

494 Lamert H, Geistlinger H, Werban U, Schutze C, Peter A, Hornbruch G, Schulz A, Pohlert M,
495 Kalia S, Beyer M, Grobmann J, Dahmke A, Dietrich P (2012) Feasibility of geoelectrical

496 monitoring and multiphase modeling for process understanding of gaseous CO₂ injection
497 into a shallow aquifer, *Environmental Earth Sciences*, vol. 67, no. 2, pp. 447–462

498 Liu Q, Maroto-Valer MM (2011) Investigation of the effect of brine composition and pH buffer
499 on CO₂-brine sequestration. *Energy Procedia* 4, 4503–4507

500 Liu Z, Moysey SM (2012) The Dependence of Electrical Resistivity-Saturation Relationships on
501 Multiphase Flow Instability. *ISRN Geophysics*, doi:10.5402/2012/270750

502 Mariyamma PN, Yan S, Tyagi RD, Surampalli RY, Zhang TC (2015) CO₂ sequestration and
503 leakage. Dans: Surampalli. In: Zhang RY, Tyagi TC, Naidu RD, Gurjar R, Ojha BR, Yan
504 CSP, Brar S, Ramakrishnan SK, Et Kao A (eds) *Carbon capture and storage: physical,*
505 *chemical, and biological methods*. American Society of Civil Engineers (ASCE), Reston,
506 pp 113–157

507 Matter JM, Kelemen PB (2009) Permanent storage of carbon dioxide in geological reservoirs by
508 mineral carbonation. *Nature Geoscience*, 2(12), pp.837–841. Available at:
509 <http://dx.doi.org/10.1038/ngeo683>

510 Metz B, Davidson O, Coninck H, Loos M, Meyer L (2005) *IPCC special report on carbon*
511 *dioxide capture and storage*, Intergovernmental Panel on Climate Change, Geneva
512 (Switzerland). Working Group III. Cambridge University Press

513 Or D, Wraith JM (1999) Temperature effects on soil bulk dielectric permittivity measured by
514 time domain reflectometry: A physical model. *Water Resour.* 35, 371–383

515 Pentland CH, El-Maghraby R, Iglauer S, Blunt MJ (2011) Measurements of the capillary
516 trapping of supercritical carbon dioxide in Berea sandstone. *Geophys Res Lett* 38(6).
517 doi:10.1029/2011GL046683

- 518 Petrik C, Mabee SB (2011) Experimental summarizing the potential of CO₂ sequestration in the
519 basalts of Massachusetts-Final report prepared for Massachusetts Clean Energy Center,
520 Boston. [http://www.geo.
521 umass.edu/stategeologist/Products/reports/BasaltSequestrationReport.pdf](http://www.geo.umass.edu/stategeologist/Products/reports/BasaltSequestrationReport.pdf). Accessed 25
522 July 2016
- 523 Plan L (2005) Factors controlling carbonate dissolution rates quantified in a field test in the
524 Austrian alps, *Geomorphology*, 68, pp. 201–212
- 525 Plug WJ, Moreno LM, Bruining J, Slob EC (2007) Simultaneous measurement of capillary
526 pressure and dielectric constant in porous media. *Piers Online* 3(4):549–553.
527 [doi:10.2529/PIERS060907154242](https://doi.org/10.2529/PIERS060907154242)
- 528 Schmidt-Hattenberger C, Bergmann P, Kießling D, Krüger K, Rücker C, Schütt H, Group K
529 (2011) Application of a Vertical Electrical Resistivity Array (VERA)for monitoring CO₂
530 migration at the Ketzin site: first performance evaluation.*Energy Proc.* 4, 3363–3370,
531 <http://dx.doi.org/10.1016/j.egypro.2011.02.258>
- 532 Scudiero E, Berti A, Teatini P, Morari F (2012) Simultaneous monitoring of soil water content
533 and salinity with a low-cost capacitance-resistance probe. *Sensors (Switzerland)*, 12(12),
534 17588–17607. <http://doi.org/10.3390/s121217588>
- 535 Snæbjörnsdóttir SO, Gislason SR (2016) CO₂ storage potential of basaltic rocks offshore
536 Iceland. The 8th Trondheim Conference on CO₂ Capture, Transport and Storage. *Energy*
537 *Procedia* 86, 371 – 380
- 538 Snæbjörnsdóttir SO, Wiese W, Fridriksson T, Armansson H, Einarsson GM, Gislason, SR

- 539 (2014) CO₂ storage potential of basaltic rocks in Iceland and the oceanic ridges. *Energy*
540 *Procedia* 63, 4585 – 4600
- 541 Shalek KJ (2013) Geophysical Numerical Modeling Approach for Characterizing and
542 Monitoring Potential Carbon Sequestration Injection Sites (PhD thesis). The Ohio State
543 University. [https://etd.ohiolink.edu/rws_](https://etd.ohiolink.edu/rws_etd/document/get/osu1366038368/inline)
544 [etd/document/get/osu1366038368/inline](https://etd.ohiolink.edu/rws_etd/document/get/osu1366038368/inline).
Accessed 19 July 2016
- 545 Socolow R, Hotinski R, Greenblatt JB, Pacala S (2004) Solving the climate problem;
546 Technologies available to curb CO₂ Emissions. *Environ. Sci. Policy Sustain. Dev.* 46, 8–19
- 547 Terzi K, Aggelopoulos CA, Bountas I, Tsakiroglou CD (2014) Effects of carbon dioxide on the
548 mobilization of metals from aquifers. *Environ. Sci. Technol.* 48, 4386–4394
- 549 Wagner FM (2016) New developments in electrical resistivity imaging with applications to
550 geological CO₂ storage. PhD Thesis, ETH-Zürich. [http://dx.doi.org/10.3929/ethz-a-](http://dx.doi.org/10.3929/ethz-a-010636965)
551 [010636965](http://dx.doi.org/10.3929/ethz-a-010636965)
- 552 Wang L, Mao Z, Shi Y, Tao Q, Cheng Y, Song Y (2014) A novel model of predicting Archie's
553 cementation factor from nuclear magnetic resonance (NMR) logs in low permeability
554 reservoirs. *Journal of Earth Science*, 25(1), 183–188. [http://doi.org/10.1007/s12583-014-](http://doi.org/10.1007/s12583-014-0411-0)
555 [0411-0](http://doi.org/10.1007/s12583-014-0411-0)
- 556 Wang S, Tokunaga TK (2015) Capillary pressure - saturation relations for supercritical CO₂ and
557 brine in limestone/dolomite sands: Implications for geologic carbon sequestration in
558 carbonate reservoirs. *Environ. Sci. Technol.*, 2015, 49 (12), pp 7208–7217. DOI:
559 [10.1021/acs.est.5b00826](https://doi.org/10.1021/acs.est.5b00826)
- 560 Zhang F (2013) Quantifying the seismic response of underground structures via seismic full

561 waveform inversion: experiences from case studies and synthetic benchmarks. Acta
562 Universitatis Upsaliensis. Digital Comprehensive Summaries of Uppsala Dissertations
563 from the Faculty of Science and Technology 1005, Uppsala, p 62Zuo L, Benson SM
564 (2014) Process-dependent residual trapping of CO₂ in sandstone.
565 Geophysical Research Letters, 41(8), 2820-2826
566 Zuo L, Benson SM (2014) Process-dependent residual trapping of CO₂ in sandstone. Geophys
567 Res Lett 41(8): 2820–2826

568

569